Transient micromixing: examples of laminar and chaotic stirring

James P. Gleeson
Applied Mathematics, University College Cork, Cork, Ireland; j.gleeson@ucc.ie

Abstract

The efficiency of a micromixing device may be quantified by the time taken for a given initial state of separated fluids to reach a desired level of homogenization. In the physically relevant case of high Peclet number the accurate prediction of the mixing time is a challenging problem, even in simple two-dimensional flows within bounded domains. In this paper a closed-form solution for the time-dependence of mixing in an annular micromixer is derived and verified by numerical simulation. The mixing time is found to scale with Peclet number as a power-law, but the power-law exponent depends on the level of homogeneity desired in the final state. Numerical simulation of a recent model of chaotic mixing reveals a vortex-like stirring effect in quasiperiodic islands of the Poincare map of the flow, which strongly influences the mixing time. This stirring effect is identified with an exponential decrease in solute variance on an intermediate timescale, being subdominant to the asymptotic long-time decay, but sensitive to the initial loading of fluids in the mixer. The subdominant decay rate is calculated to scale with Peclet number as the square root of the dominant decay rate.

PACS: 47.85.-g; 05.45.-a; 47.52.+j

1 Introduction

Efficient mixing of fluids in channels with dimensions on the order of microns is vital to the operation of lab-on-a-chip technology, micro total analysis systems (μTAS), and other microfluidic devices. With characteristic length scales of 100 microns or less, and flow speeds on the order of millimeters per second, the Reynolds numbers of such flows are typically quite small. In this Stokes-flow regime, the fluid velocity is smooth and laminar. The lack of turbulence implies that the common macroscale mixing by eddies and whorls (seen, for instance, when stirring cream into coffee) is absent in such microfluidic devices. Mixing by diffusion relies upon the random motion of molecules across the interface between the fluids, and the time required for mixing by diffusion alone is typically too long to be of interest to users of the end technology. Consequently, significant recent research effort has been invested in finding methods to quantify and accelerate micromixing. For example, annular micromixers such as that depicted schematically in Figure 1 have been tested by a number of groups. The fluids to be mixed are loaded into the annular space between concentric cylindrical walls, and then pumped around the annulus by peristaltic pumps [1] or using magnetohydrodynamic (MHD) forces [2] upon the fluids. The velocity of the fluids is zero at the inner and outer walls, with a maximum near the center of the channel. Consequently the lamellae of solute and solvent are stretched and interwoven (Figure 1(c)) by the convection process, and the interface length between the fluids is lengthened so that the diffusive mixing is significantly accelerated.

The importance of the convective stirring mechanism relative to the molecular diffusion in a given mixing problem is measured by a nondimensional number called the Peclet number, defined as

$$Pe = \frac{UL}{D}. \tag{1}$$

Here U is a typical flow speed in the device, L is a characteristic length scale, and D is the molecular diffusivity. Most cases of interest have very large Peclet numbers, with typical values in the range 10^3 to 10^5. Physically this implies that the stretching of the fluid interface by convection proceeds for a substantial amount of time before diffusive effects eventually smear out the interface and mix the fluids at small lengthscales. Large Pe values also render the numerical solution of the convection-diffusion equation extremely challenging.

The mixer depicted in Figure 1 stretches the fluid interface with each revolution of the fluid around the annulus. Stretching of this sort leads to a linear growth of the total interface length with time, and is termed laminar mixing. It is clear that much faster mixing may be achieved if the interface between the fluids can be stretched at a faster rate. Chaotic mixing devices aim to achieve exponential growth of the total interface length in time by stretching and folding the fluids in a similar fashion to the transformation maps of chaotic dynamics theory [3]. Of course the final mixing of the fluids is still governed by the action of diffusion [4]. Micromixers incorporating chaotic mixing have been constructed recently, see [5] for example, and the review article [6].

It is useful to have a quantitative measure of the efficiency of mixing in a given device in order to compare various designs and predict the times required for mixing-dependent process steps. The length of the interface between the fluids provides an initial estimate of mixing efficiency, but the interface becomes blurred as diffusion acts. Moreover, it is possible that significant regions of the fluid remain unmixed despite the stretching and folding of the fluid interface in other regions of the device. Accordingly, we choose to quantify mixing efficiency by a mixing measure $m(t)$ which is defined as the variance of the concentration of one of the fluids over the whole domain of the device, see equation (5) below. Thus, in the presence of non-zero diffusion, $m(t)$ decreases with time t from its initial value towards the fully mixed homogeneous state corresponding to $m = 0$. The rate of decay of $m(t)$ is of obvious interest to micromixer designers, but in general its prediction by standard numerical methods is difficult owing to the typically high Peclet number. We note here that the definition of the mixing measure as the variance of the concentration throughout the device domain implies that we consider only closed domains, such as are typical of engineering devices. Mixing and effective diffusivity in infinite spaces have been examined by homogenization methods [7], but a different approach is required in closed domains [8].

Most work on characterizing the decay of $m(t)$ in closed domains has concentrated on the long-time limit $t \to \infty$. In the two-dimensional cases we consider here, the mixing measure is found to eventually decay exponentially:

$$m(t) \sim \exp(-\lambda_1 t) \text{ as } t \to \infty, \tag{2}$$

with the decay rate λ_1 scaling with large Peclet number as

$$\lambda_1 \sim Pe^{-\alpha} \text{ as } Pe \to \infty. \tag{3}$$

Mixing by the action of diffusion alone corresponds to $\alpha = 1$; Giona et al. [9] have shown that a wide class of unidirectional flows in periodic domains give a convection-enhanced diffusion with $\alpha = 1/2$. In models of chaotic mixing, α has been found to take various values between 0 and 1, depending upon the eigenfunction structure of the given mixing operator [10].

In this paper we focus attention on the transient behavior of $m(t)$, i.e., its rate of decay for times prior to those where the asymptotic limit (2) applies, in two examples of model micromixers. In section 3 we find the full time-dependent function $m(t)$ for laminar annular mixers where the stirring is due to, e.g., magnetohydrodynamic forces, and in the physically relevant asymptotic limit of small curvature effects. In our second example (section 4), we examine the time dependence of $m(t)$ in a chaotic mixer model using numerical simulations. We demonstrate a sub-dominant exponential decay of $m(t)$ which depends upon the initial loading of the fluids into the micromixer and identify the underlying physical mechanism of 'stirring' in persistent Kolmogorov-Arnold-Moser (KAM) islands of the chaotic map. Although this stirring

effect is subdominant to (2) in the long-time limit, it is likely to be very relevant to engineers seeking to maximize the mixing of fluids within a finite time. Our two examples are chosen to illustrate that stirring (or 'stirring-like') effects can have important consequences for the transient mixing measure $m(t)$ in models of both laminar (section 3) and chaotic (section 4) micromixing.

2 Mathematical formulation

The mixing of two fluids of similar physical properties (density, viscosity, etc.) is described by the convection-diffusion equation

$$\frac{\partial c}{\partial t} + \mathbf{v} \cdot \nabla c = D \nabla^2 c, \tag{4}$$

with suitable initial and boundary conditions. Here $c(\mathbf{x}, t)$ is the concentration of one of the fluids (the solute) as a function of position $\mathbf{x}$ within the mixer, and of time t. The molecular diffusion is described by the diffusivity constant D, and convection is due to the divergence-free velocity field $\mathbf{v}(\mathbf{x}, t)$ of the incompressible fluid flow. Note the divergence-free property of the velocity field justifies the form of the advection term in (4), since $\nabla \cdot (\mathbf{v}c) = \mathbf{v} \cdot \nabla c$. The fluid velocity may be found by solving the Navier-Stokes equations with suitable forcing terms, however in many cases the velocity $\mathbf{v}$ is assumed to have some simple analytical form in order to clarify the interplay of the processes involved in mixing. The physical picture described by (4) is of solute being passively convected with the local fluid velocity $\mathbf{v}$, and diffused by molecular diffusion. Solutions of this equation enable us to quantify the simple arguments advanced in section 1 for the speed of mixing in a given micromixer design.

Equation (4) is to be solved in a closed domain representing the micromixer geometry — we consider only two-dimensional examples in this paper. Boundary conditions at the device walls are typically no-flux, i.e., Neumann conditions. The initial condition $c(\mathbf{x}, 0)$ specifies the initial loading of the solute in the mixer; we show in section 4 how careful initial loading can strongly affect the mixing time. Given the initial and boundary conditions, equation (4) can be solved for $c(\mathbf{x}, t)$, usually requiring high-resolution numerical methods. For simple boundary conditions, the homogeneous state with c being constant everywhere is a solution of (4) and corresponds to the steady-state limit $t \to \infty$ of the solution $c(\mathbf{x}, t)$. The *mixing measure* $m(t)$ is defined as

$$m(t) \equiv \left\langle c^2 \right\rangle - \left\langle c \right\rangle^2, \tag{5}$$

where the angle brackets denote averaging over the mixer, i.e., integrating over the spatial domain. The mixing measure thus gives the variance of the concentration over the mixer, and (in the presence of non-zero diffusion) decreases with time from its initial value. In the final homogeneous state $c = \langle c \rangle$, and so the mixing measure reaches zero in the steady state limit. Note the importance of the diffusion term in (4) to this definition of mixing measure — indeed in the absence of diffusion the measure $m(t)$ would remain identically constant and equal to its initial value. As discussed in section 1, the rate of decay of $m(t)$ provides important information for designers and users of micromixers. For example, a natural question to ask is "how long does this mixer take to reduce the initial loading to a given value M of $m(t)$?" This defines a *mixing time* T_M to reach a required level of mixing M:

$$m(T_M) = M. \tag{6}$$

In section 3 we show that the scaling of T_M with Peclet number depends on how finely mixed an end product is desired.

3 Laminar mixing

In this section we examine mixing in laminar, non-chaotic flows; in particular concentrating on micromixers in the form of an annulus. In section 3.2 we briefly review the results of [11] on mixing at the center of smooth vortices.

3.1 Annular micromixer

Micromixers with annular geometries as in such as Figure 1 have been constructed and tested by a number of groups. The Quake group [1] use a peristaltic pumping mechanism to drive the fluids around the channel. In [2, 12] a magnetohydrodynamic (MHD) pumping mechanism is shown to provide a steady pumping force around the annulus. The two-dimensional modelling of this problem has been considered in [13], including detailed analysis of the low and intermediate (Taylor dispersion) Peclet number cases; here we concentrate on the high Peclet number regime.

The polar coordinate system for this device is described in Figure 2: the radius of the center of the channel is R, and ρ is the half-width of the channel. Thus the inner wall is located at $r = R - \rho$ and the outer wall at $r = R + \rho$. The nondimensional parameter

$$\gamma = \frac{\rho}{R} \tag{7}$$

is used to specify the mixer design; note $0 < \gamma < 1$, with the $\gamma \to 0$ limit corresponding to a locally straight (zero curvature) channel. Solving the two-dimensional Navier-Stokes equations with a constant body force gives the fluid velocity $\mathbf{v}$ [13]. The streamlines are circles, with angular speed

$$v(r) = \frac{\beta}{8R\rho r}\left[(R^2-\rho^2)^2 \ln\frac{R-\rho}{R+\rho} + r^2(R-\rho)^2 \ln\frac{r}{R-\rho} + r^2(R+\rho)^2 \ln\frac{R+\rho}{r}\right], \tag{8}$$

where the constant β represents the MHD body force, see [13] for details. This profile reduces to the parabolic Poiseuille profile for a straight channel in the limit $\gamma \to 0$:

$$v(r) \approx \frac{3\omega R}{2\rho^2}(r - R + \rho)(R + \rho - r) \tag{9}$$

where the average angular velocity ω has been defined as:

$$\omega = \beta\left[\frac{1}{4} - \frac{(R^2-\rho^2)^2}{16R^2\rho^2}\left(\ln\frac{R-\rho}{R+\rho}\right)^2\right]. \tag{10}$$

The convection-diffusion equation (4) for the solute concentration $c(r, \phi, t)$ in the polar coordinate system is

$$\frac{\partial c}{\partial t} + \frac{v(r)}{r}\frac{\partial c}{\partial \phi} - \frac{D}{r}\frac{\partial}{\partial r}\left(r\frac{\partial c}{\partial r}\right) - \frac{D}{r^2}\frac{\partial^2 c}{\partial \phi^2} = 0, \tag{11}$$

with no-flux boundary conditions at the walls:

$$\begin{aligned} \frac{\partial c}{\partial r}(R-\rho, \phi, t) &= 0 \\ \frac{\partial c}{\partial r}(R+\rho, \phi, t) &= 0. \end{aligned} \tag{12}$$

The Peclet number is defined for this system as

$$Pe = \frac{\omega R \rho}{\kappa}. \tag{13}$$

Note that ωR is the characteristic linear velocity, while ρ is the smallest linear dimension in the system.

The geometry of the annulus means that the concentration $c(r, \phi, t)$ must be periodic in the angle ϕ, and so a Fourier series representation may be used. Indeed from equation (11) it is easy to see that the angular Fourier modes are uncoupled, thus simplifying both numerical and analytical solutions. Numerical results for the simple initial condition

$$c(r, \phi, 0) = \cos \phi \tag{14}$$

and $\gamma = 0.05$ are shown in Figures 3 and 4. Figure 3 presents logarithmic plots of $m(t)$, normalized so $m(0) = 1$. For Peclet numbers up to about 100 the decay of $m(t)$ is exponential in time, as evidenced by the straight lines in Fig. 3(a). For higher Pe however, distinctly non-exponential sections are seen in the early part of the $m(t)$ curve (Fig. 3(b)), with a final decay which is exponential in time. The mixing time T_M to reach a mixing level M as defined in (6) is shown in Fig. 4 for three different values of M: 0.3, 0.1, and 0.01, and is plotted as a function of Peclet number. Note that the time T_M is normalized here by the average rotation time $1/\omega$. In previous work [13] we have shown that the $Pe < 100$ region can be described using the concept of Taylor dispersion; here we concentrate on the $Pe \gg 100$ region. For high Peclet numbers and $M = 0.3$ or 0.1, the nondimensional time to mix appears to scale as Pe^{α}, with $\alpha = 1/3$. However when a higher level of homogeneity is demanded ($M = 0.01$ case), a different scaling emerges, with $\alpha = 1/2$. To understand the behavior seen in these figures we require a detailed asymptotic analysis of the convection-diffusion equation.

Numerical simulations indicate that the stretching and subsequent diffusive mixing of lamellae is most effective near the walls of the channel. A persistent structure which mixes more slowly than the rest of the solute is located near the center of the channel, where the angular velocity (9) reaches its maximum. A related phenomenon is identified by Giona et al. [9] for mixing due to a unidirectional flow in a periodic domain: they identify the quadratic maximum of $v(r)$ as leading to a persistent structure with an exponential decay rate (related to $1/T_M$) scaling as $Pe^{-1/2}$. Motivated by the numerical results and the localized eigenfunctions identified in [9], we focus on the center of the channel by making the change of variable

$$\begin{aligned} \tilde{r} &= \frac{r - R}{\rho}, \\ \tilde{t} &= \omega t. \end{aligned} \tag{15}$$

and taking the asymptotic limit $\gamma \to 0$. Note the nondimensional radial variable $\tilde{r}$ lies between -1 and 1, with $\tilde{r} = 0$ in the center of the channel. Taking the limit of small γ and using (9), equation (11) reduces to

$$\frac{\partial c}{\partial \tilde{t}} + \frac{3}{2}\left(1 - \tilde{r}^2\right) \frac{\partial c}{\partial \phi} - \epsilon \frac{\partial^2 c}{\partial \tilde{r}^2} = 0, \tag{16}$$

where $\epsilon = (\gamma Pe)^{-1}$ is a small parameter when Pe is sufficiently large. We follow [11] and [14] in seeking a solution of (16) of the form

$$c = g(\tilde{t}) \exp\left[in\phi - \frac{3}{2} in\tilde{t} - if(\tilde{t})\tilde{r}^2\right], \tag{17}$$

where the functions $g(\tilde{t})$ and $f(\tilde{t})$ are to be determined, subject to initial conditions $g(0) = 1$, $f(0) = 0$. Remarkably, $f(\tilde{t})$ and $g(\tilde{t})$ can be found so that (17) is an *exact* solution of (16). Substituting (17) into

(16) and taking $n = 1$ for the initial condition (14), we find first-order equations for f and g:

$$\begin{aligned} \frac{df}{d\tilde{t}} &= -4i\epsilon f^2 - \frac{3}{2}, \\ \frac{dg}{d\tilde{t}} &= -2i\epsilon fg. \end{aligned} \tag{18}$$

The solution of this nonlinear system satisfying the initial conditions is

$$\begin{aligned} f(\tilde{t}) &= \frac{3(1+i)}{2}\frac{1}{\mu}\tanh\left(\frac{-1+i}{2}\mu\tilde{t}\right), \\ g(\tilde{t}) &= \left[\cosh\left(\frac{-1+i}{2}\mu\tilde{t}\right)\right]^{-\frac{1}{2}}, \end{aligned} \tag{19}$$

where we have written $\mu = 2\sqrt{3\epsilon}$ for clarity of presentation. After some manipulation, using (17) in (5) yields the full time-dependence of the mixing measure:

$$m = \sqrt{\frac{\pi}{6}}\mu\left[\sinh(\mu\tilde{t}) - \sin(\mu\tilde{t})\right]^{-\frac{1}{2}}\operatorname{erf}\left[\sqrt{\frac{3}{\mu}}\sqrt{\frac{\sinh(\mu\tilde{t}) - \sin(\mu\tilde{t})}{\cosh(\mu\tilde{t}) + \cos(\mu\tilde{t})}}\right]. \tag{20}$$

To understand the implications of this rather complex expression, we examine various limiting cases. When $\mu\tilde{t} \ll 1$, the result reduces to

$$\begin{aligned} m &\approx \sqrt{\frac{\pi}{2}}\left(\mu^2\tilde{t}^3\right)^{-\frac{1}{2}}\operatorname{erf}\left[\frac{1}{\sqrt{2}}\left(\mu^2\tilde{t}^3\right)^{\frac{1}{2}}\right] \\ &= \frac{\sqrt{\pi}}{2}F\left(\frac{6\omega^3t^3}{\gamma Pe}\right), \end{aligned} \tag{21}$$

where F is defined as the monotonic function

$$F(x) = x^{-1/2}\operatorname{erf}(x^{1/2}). \tag{22}$$

The nondimensional mixing time corresponding to a mixing measure value of M is therefore

$$\omega T_M \approx \left[\frac{\gamma Pe}{6}F^{-1}\left(\frac{2M}{\sqrt{\pi}}\right)\right]^{1/3}, \tag{23}$$

and note in particular that this increases as $Pe^{1/3}$ when M and γ are fixed.

For $\mu\tilde{t} \gg 1$, the solution (20) decays exponentially in time:

$$m \approx \sqrt{\frac{\pi}{3}}\mu\operatorname{erf}\left[\sqrt{\frac{3}{\mu}}\right]\exp\left[-\frac{1}{2}\mu\tilde{t}\right], \tag{24}$$

and for large Peclet numbers $\mu \ll 1$, so the asymptotic mixing time is given (in dimensional variables) by

$$\omega T_M \approx \frac{1}{4}\sqrt{\frac{\gamma Pe}{3}}\ln\left[\frac{4\pi^2}{3M^4}\frac{1}{\gamma Pe}\right]. \tag{25}$$

Note that this mixing time scales as $Pe^{1/2}\ln Pe$ for fixed M and γ. This longer timescale replaces the $Pe^{1/3}$ scaling given by (23) when the mixing time T_M is sufficiently large that the $\mu\tilde{t} \gg 1$ asymptotics

are important—this is relevant when we seek a level of mixing M that is sufficiently small. Physically, this new scaling emerges as a consequence of the vanishing of the differential rotation rate at the center of the channel: $v'(0) = 0$, see [11] for a detailed discussion of the analogous problem at vortex centers. Over short timescales (with $\mu\tilde{t} \ll 1$), the advective stretching and diffusion mix the scalar with time scaling as $Pe^{1/3}$. This convection-enhanced mixing is most effective near the sides of the channel, where the scalar is stretched into thin lamellae, see Figure 1(c). The more persistent scalar structure at the center of the channel is only destroyed on the longer timescales ($\mu\tilde{t} \gg 1$), leading to the $Pe^{1/2} \ln Pe$ scaling in (25). It is noteworthy that (17) does not satisfy the no-flux boundary conditions (12) at the walls of the channel. However, numerical simulations indicate that this does not have an appreciable effect upon the accuracy of the asymptotic formulas. This is a consequence of the fast mixing of the scalar near the walls, so that any error in the boundary conditions is dominated by the slower-mixing scalar structure in the channel center.

3.2 Persistent structures in vortex mixing

Bajer et al. [11] have recently performed a similar asymptotic analysis to that discussed above, but in the context of mixing in an isolated two-dimensional vortex. They find that the time-dependence of the mixing is dominated by the persistent structure at the (smooth) vortex center and conclude that in the long-time limit, $m(t)$ decays exponentially in time, with a rate which scales as $Pe^{-1/2}$.

A rate scaling as $Pe^{-1/2}$ has also been found in a two-dimensional chaotic mixing flow by Cerbelli et al. [15]. The flow considered in [15] has chaotic mixing regions, but its Poincare section is dominated by large quasiperiodic islands. A numerical study of the mixing rate shows that the decay of $m(t)$ at intermediate times is exponential with a $Pe^{-1/2}$ rate, but at later times mixing slows to an exponential with a Pe^{-1} rate. In the next section we discuss an interpretation of this result as due to a stirring-like action within the quasiperiodic islands of the chaotic flow. We hypothesize that the stirring effect can be important in the transient behavior of $m(t)$, even when islands do not dominate the mixing flow. An example of such a chaotic mixing scheme based on the standard map is presented in the next section. Calculation of $m(t)$ over time requires extensive numerical simulation, and exponential decay rates are found by fitting numerical data. The physical picture of stirring within islands proves extremely useful in interpreting the results of mixing in chaotic flows, particularly their dependence upon the initial condition, i.e., the manner in which solute and solvent are loaded into the micromixer, and are thus of immediate interest to micromixer designers.

4 Chaotic mixing

The mixing properties of chaotic flows (in the absence of diffusion) have attracted much interest, both mathematical [3] and experimental [5]. Recent work [10] has focused on the interplay of diffusion with flows which are not globally chaotic, but contain quasiperiodic islands in their Poincare section. Giona et al. [10] examine the effects of two-dimensional, time-periodic velocity fields in equation (4), with the domain being periodic in both x and y directions, i.e., a torus. It is well-established that the resulting mixing measure $m(t)$ decays exponentially as $t \to \infty$, with a rate that is given the appropriate eigenvalue of the Poincare operator [10]. This eigenvalue is found to scale with Peclet number as $Pe^{-\alpha}$, with the value of $\alpha \in (0, 1]$ being characteristic of the flow field.

A recent paper [15] has also shown that another, sub-dominant exponential decay rate can be seen in $m(t)$ at intermediate times, i.e., before the long-time limit dominates. In a chaotic flow which is dominated by quasiperiodic islands (KAM curves) certain initial conditions show a subdominant decay rate scaling as $Pe^{-1/2}$, which persists until the dominant decay rate (scaling diffusively as Pe^{-1}) makes itself felt. Contour plots of the concentration show that the interior of each individual KAM island appears to have

a stirring effect, qualitatively similar to that seen in the vortex mixing described in section 3.2. Moreover, the scaling of the $Pe^{-1/2}$ rate matches the persistent vortex mixing rate found by Bajer et al. After all islands have internally homogenized, the final (global) mixing proceeds by diffusion between the islands in an effort to reduce the concentration variance until the concentration is uniform everywhere in the domain. This diffusive rate scales as Pe^{-1}.

Despite the similar scaling seen in vortex mixing and island 'stirring', we stress that there are important differences between the two flows: for instance, the vortex studied by Bajer et al. is steady, while the time periodic sine flow used by Cerbelli et al. is defined as the periodic sequence of two steady sinusoidal flows. We are thus motivated to investigate whether a stirring-like mechanism can be found in other chaotic mixing flows, and to examine the scaling of the exponential decay rates.

Pikovsky and Popovych [4] recently examined mixing by a time-periodic flow on a torus by splitting the operators of advection and diffusion. Specifically, the time-periodic flow is driven by the periodic alternation of two perpendicular flows: $\mathbf{v}_1 = (y, 0)$ for time interval t_1, and $\mathbf{v}_2 = (0, c\sin(x))$ for time interval $t_2 = K/c$, with overall period $T = t_1 + t_2$ taken to be unity. In the absence of diffusion, the position (x_n, y_n) of a tracer at time intervals $t = nT$ is given by the standard map

$$\begin{aligned} x_{n+1} &= (x_n + y_n) \mod 2\pi \\ y_{n+1} &= (y_n + K\sin(x_{n+1})) \mod 2\pi, \end{aligned} \tag{26}$$

where the constant K is chosen to be 4. Pikovsky and Popovych show that the probability density for the noisy standard map, or equivalently the solute concentration when diffusion acts only in 'pulses' at times nT, is evolved by the Frobenius-Perron operator [4]. The resulting concentration at iteration n can be found from the equation for its Fourier transform [4]

$$\psi_{n+1}(l,q) = \exp\left(-\frac{l^2+m^2}{P}\right)\sum_j \psi_n(j, q+j)J_{j-l}(qK), \tag{27}$$

where the Fourier transform is

$$\psi_{n+1}(l,q) = \frac{1}{4\pi^2}\int_0^{2\pi} dx \int_0^{2\pi} dy\, c(x,y,n)\, e^{-i(lx+qy)}. \tag{28}$$

Here $J_n(k)$ are Bessel functions, and P is inversely proportional to the diffusivity and so plays the role of a Peclet number. By maintaining a finite number of modes (up to 401×401) in (27) we get a numerical approximation to the concentration density, and hence to the mixing measure $m(n)$ at each iteration.

It is important to note that the applicability of such a 'pulsed' system to the continuous-in-time convection-diffusion equation (4) is matter of considerable debate. The pulsed diffusion can be viewed as a mollification of the Frobenius-Perron operator associated with pure advection in order to make it compact, and thus considerably simplify numerical simulations. However the actual physics of the problem is correctly captured by solving the full advection-diffusion problem for the original time-periodic flow field (as performed for a different flow in [8, 15]). The physical relevance of the pulsed approach has therefore been questioned by some authors [8]. Nevertheless, we follow [4] in using such a system in order to highlight the fact that the stirring mechanism responsible for important transient behavior of $m(t)$ occurs even in a simplified chaotic mixing example.

A Poincare section of the standard map is shown in Figure 5 — note the quasiperiodic island, surrounded by a chaotic mixing sea. To highlight the role of the island we choose two different initial conditions (see the dashed and solid rectangles overlaid on Fig. 5). Condition 1 (dashed rectangle) consists of a horizontal band of solute (with $c = 1$ within the band, $c = 0$ elsewhere) which traverses the quasiperiodic island;

condition 2 (solid rectangle) is a vertical band of same volume and density, but situated so that it mostly avoids intersecting the island. The concentration density after a number of iterations is shown in Figure 6: in each picture the greyscale intensity varies from black (low c) to white (high c).

Condition 1 (left column) is seen to be mixed relatively quickly outside of the island, and to then mix within the island in a vortex-like fashion — note especially the 'stirred' structure in the center of Fig. 6(c) and (d). At the end of this intermediate time period (about iteration 30) the island is well-mixed, and the remaining global mixing is due to the slow decay of the dominant eigenfunction. The plot of $m(n)$ in Figure 7 shows that the stirring interval has a subdominant exponential decay rate. By contrast, condition 2 (right column of Figure 6) has almost no initial solute within the island, and so (after the fast outside mixing) the only way solute can enter the island to equalize the global concentration is by the slow diffusion process specified by the dominant eigenfunction. Note from Figure 7 that the time T_M required to reach a given level M of mixing is thus greatly reduced for condition 1: although the local stirring within the island is slower than the chaotic mixing outside, from a global viewpoint it is better to have solute homogenized throughout the island structure in order to reduce the time needed for the slow decay of the dominant eigenfunction.

Figure 8 shows the mixing measure $m(n)$ for condition 1 at various values of the Peclet number P. Exponential fits are performed to determine the decay rates, see Fig. 9. Power law scalings with P are found for both the dominant and subdominant decay rates; these are respectively $P^{-\alpha}$ and $P^{-\alpha_s}$, with $\alpha = 0.75$ and $\alpha_s = 0.37$. The difference from the scalings found in [15] (respectively $\alpha = 1$ and $\alpha_s = 1/2$) is to be expected, as the chaotic flow used here is not dominated by quasiperiodic islands. Interestingly, we cannot rule out the hypothesis that the subdominant decay rate scales as the square root of the dominant rate, i.e., $\alpha_s = \alpha/2$: simulation of other mixing systems is required for further investigation of the decay rates.

As noted above, the physical relevance of the pulsed advection-diffusion operator used here may well be questioned. Nevertheless, given that a subdominant decay was also found in the continuous-time system of [15], we anticipate that the subdominant 'stirring effect' highlighted here should also appear in solutions of the full continuous-time advection-diffusion equation for this system, and so have an important impact on the transient mixing measure. Extensive numerical simulation is required to test this prediction, and to establish the appropriate scaling exponents.

5 Conclusions

We have examined the time-dependence of a physically-relevant mixing measure in two examples of flow models in two-dimensional bounded domains. The annular micromixer design is based on experimental prototypes [1, 2], and is closely related to a recent theoretical analysis of asymptotic mixing rates in smooth flows [9]. Using a spectral method we are able to numerically simulate mixing at Peclet numbers above 10^4; moreover, asymptotic methods enable us to derive an accurate closed-form approximation for the mixing measure at all times. This analytical result explains the initially puzzling situation whereby the time to mix the fluids scales as a power of the Peclet number, with the power being 1/3 or 1/2 depending on the level of homogeneity required in the final product.

We also perform numerical simulations of a recently-introduced 'pulsed' model of chaotic mixing in the standard map [4]. The mixing mechanism of the solute within quasiperiodic islands of the Poincare map is identified as a 'stirring effect', and shown to strongly affect the dynamics of the mixing measure. During the stirring, the rate of decay of the mixing measure with time has a scaling $\sim P^{-\alpha_s}$, and is subdominant to the long-time decay rate which scales as $P^{-\alpha}$. Our results (Fig. 9) indicate that values of $\alpha_s = 0.37$ and $\alpha = 0.75$ are appropriate for the mixing model in question.

The fact that mixing in the standard map, and also in a continuous-time chaotic flow considered previously [15] both produce a stirring effect with decay rates whose P-scalings satisfy the relationship

$$\alpha_s = \frac{\alpha}{2} \tag{29}$$

is very suggestive. We speculate that an investigation of the scaling of subdominant eigenvalues of the Poincare operator (similar to that performed recently for the dominant eigenvalues [8, 10]) might yield insight into the stirring effect. Alternatively, a phenomenological approach based on the analogy with vortex mixing [11] in the presence of an effective global diffusivity $D_{\text{eff}} \sim P^{\alpha}$ may prove more useful in predicting the mixing times required in a given micromixer design.

6 Acknowledgements

This work is supported by a Science Foundation Ireland Investigator Award, under programme number 02/IN.1/IM062.

References

[1] H-P. Chou, M. A. Unger, and S. R. Quake, "A microfabricated rotary pump," Biomedical Microdevices **3:4**, 323 (2001).

[2] J. West et al., "Application of magnetohydrodynamic actuation to continuous flow chemistry," Lab on a Chip **2**, 224 (2002).

[3] J. M. Ottino, *The kinematics of mixing: stretching, chaos, and transport,* (Cambridge U.P., Cambridge, 1989).

[4] A. Pikovsky and O. Popovych, "Persistent patterns in deterministic flows," Europhys. Lett. **61**, 625 (2003).

[5] A. D. Stroock et al., "Chaotic mixer for microchannels," Science **295**, 647 (2002).

[6] H. A. Stone, A. D. Stroock, and A. Ajdari, "Engineering flows in small devices: microfluidics towards a lab-on-a-chip," Ann. Rev. Fluid Mech. **36**, 381 (2004).

[7] A. Fannjiang and G. Papanicolaou, "Convection enhanced diffusion for periodic flows," SIAM J. Appl. Math. **54**, 333 (1994).

[8] S. Cerbelli, V. Vitacolonna, A. Adrover, and M. Giona,"Eigenvalue-eigenfunction analysis of infinitely fast reactions and micromixing regimes in regular and chaotic bounded flows," Chem. Eng. Sci. **59**, 2125 (2004).

[9] M. Giona, S. Cerbelli, and V. Vitacolonna, "Universality and imaginary potentials in advection-diffusion equations in closed flows," J. Fluid Mech. **513**, 221 (2004).

[10] M. Giona, A. Adrover, S. Cerbelli, and V. Vitacolonna, "Spectral properties and transport mechanisms of partially chaotic bounded flows in the presence of diffusion," Phys. Rev. Lett. **92**, art. no. 114101 (2004).

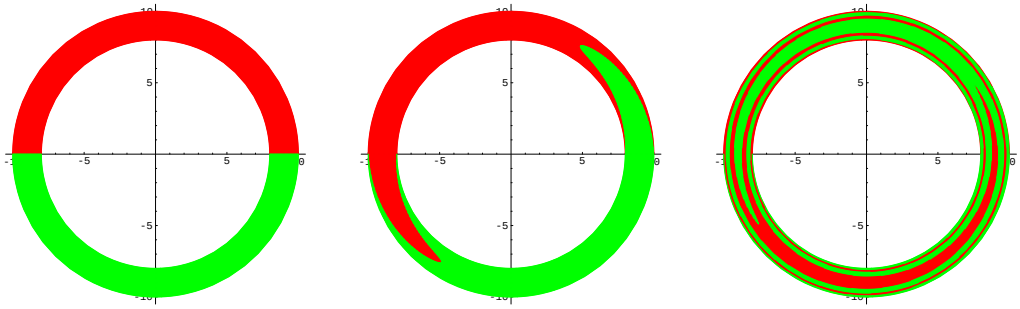

Figure 1: Operation of an idealized annular micromixer at three times.

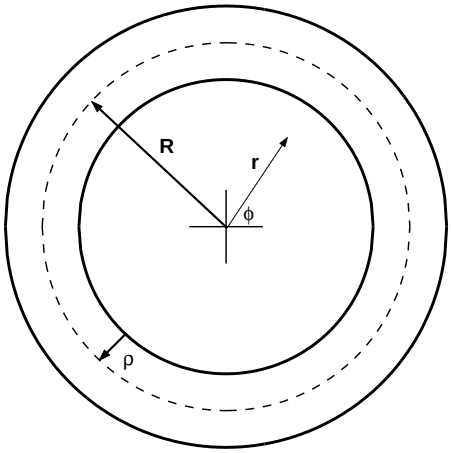

Figure 2: Annular geometry, showing the center-line radius R, and the channel half-width ρ.

[11] K. Bajer, A. P. Bassom and A. D. Gilbert, "Accelerated diffusion in the centre of a vortex," J. Fluid Mech. **437**, 395 (2001).

[12] J. P. Gleeson and J. West, "Magnetohydrodynamic Micromixing," in *Proceedings of the Fifth International Conference on Modeling and Simulation of Microsystems 2002*, 318, (Computational Publications, 2002).

[13] J. P. Gleeson, O. M. Roche, J. West, and A. Gelb, "Modelling annular micromixers," SIAM J. Appl. Math. **64**, 1294 (2004).

[14] M. J. Lighthill, "Initial development of diffusion in a Poiseuille flow," J. Inst. Maths Applics. **2**, 97 (1966).

[15] S. Cerbelli, A. Adrover, and M. Giona, "Enhanced diffusion regimes in bounded chaotic flows," Phys. Lett. **312**, 355 (2003).

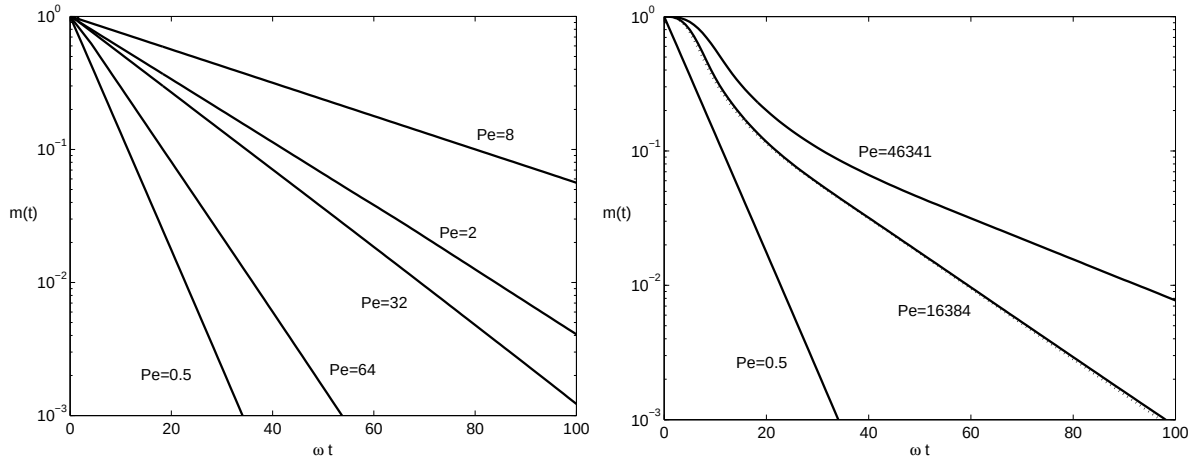

Figure 3: Mixing measure $m(t)$ as a function of nondimensional time, calculated in numerical simulations with $\gamma = 0.05$ and various Peclet numbers as shown. The asymptotic result (20) for $Pe = 16384$ is also shown with a dotted curve on the right, almost indistinguishable from the numerical result.

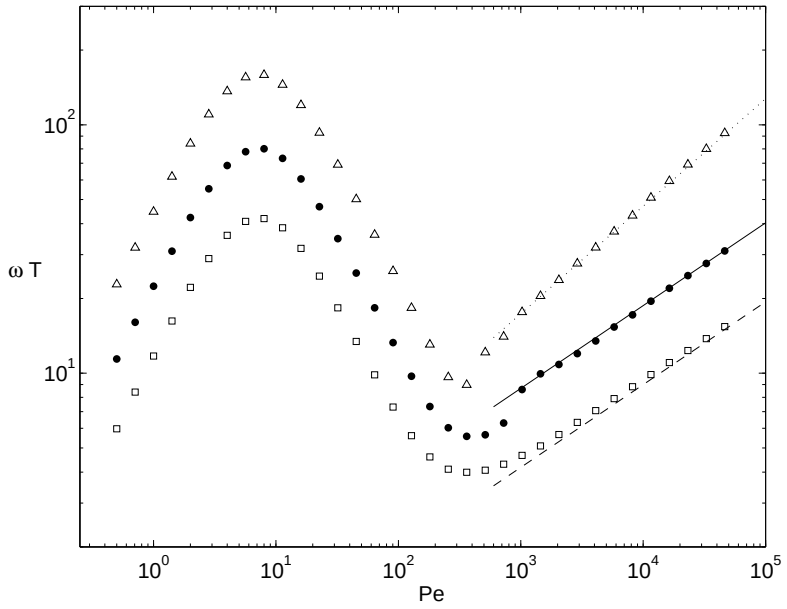

Figure 4: Nondimensional mixing times as a function of Peclet number, for $\gamma = 0.05$. Asymptotic results are shown as lines, and numerical results as symbols for values of the mixing measure: $M = 0.3$ (dashed line, squares), $M = 0.1$ (solid line, points), and $M = 0.01$ (dotted line, triangles). The asymptotic result (23) is applied to the $M = 0.3$ and $M = 0.1$ cases, while the long-time version (25) is needed in the well-mixed $M = 0.01$ situation.

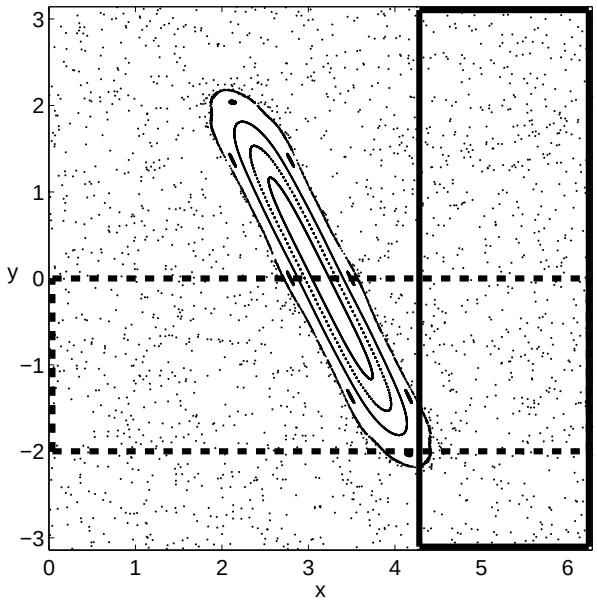

Figure 5: Poincare section of the standard map (26). Note the 2π-periodic variable y is shown over the range $[-\pi, \pi]$ to highlight the central island. Initial condition 1 of the mixing problem has the solute distributed uniformly inside the dashed rectangle, with the solid rectangle bounding initial condition 2.

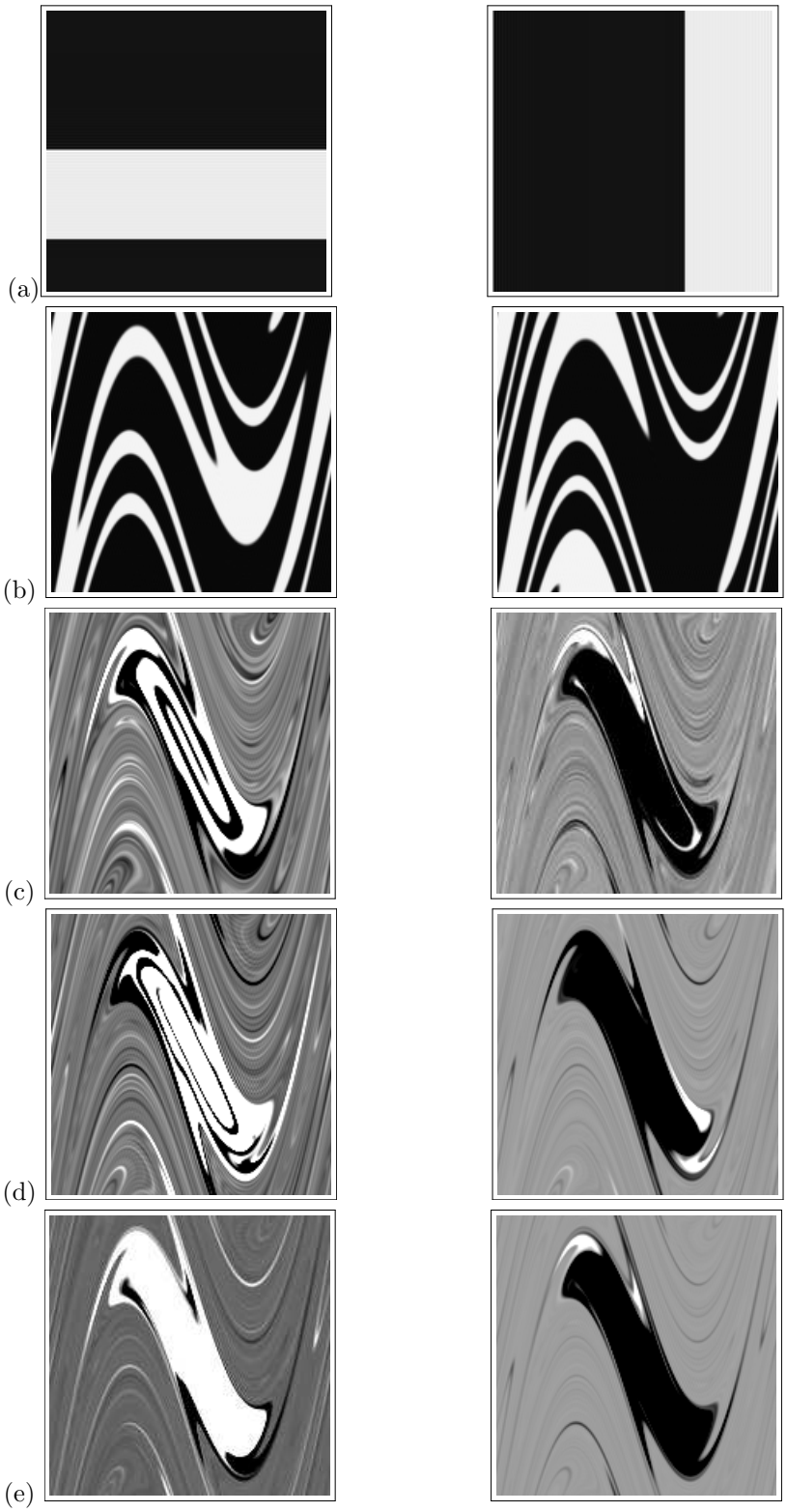

Figure 6: Concentration density for initial condition 1 (left column) and condition 2 (right column). (a) Initial conditions, (b) $n = 2$, (c) $n = 14$, (d) $n = 24$, (e) $n = 50$. The highest concentration values in each picture are white, and lowest are black. Note the stirring effect within the island in the left column of (c) and (d).

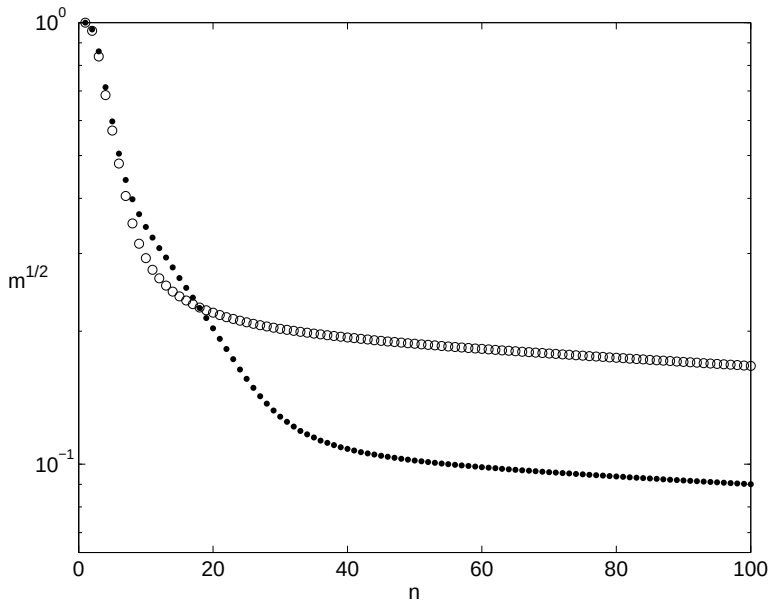

Figure 7: Mixing measure $m(n)$ for the noisy standard map. Filled symbols are for initial condition 1 (which intersects the quasiperiodic island); open circles are for initial condition 2. Note the exponential decay of condition 1 between $n = 10$ and $n = 30$ — the rate of decay is faster than (subdominant to) the final exponential decay, but nevertheless has a strong impact on the mixing measure.

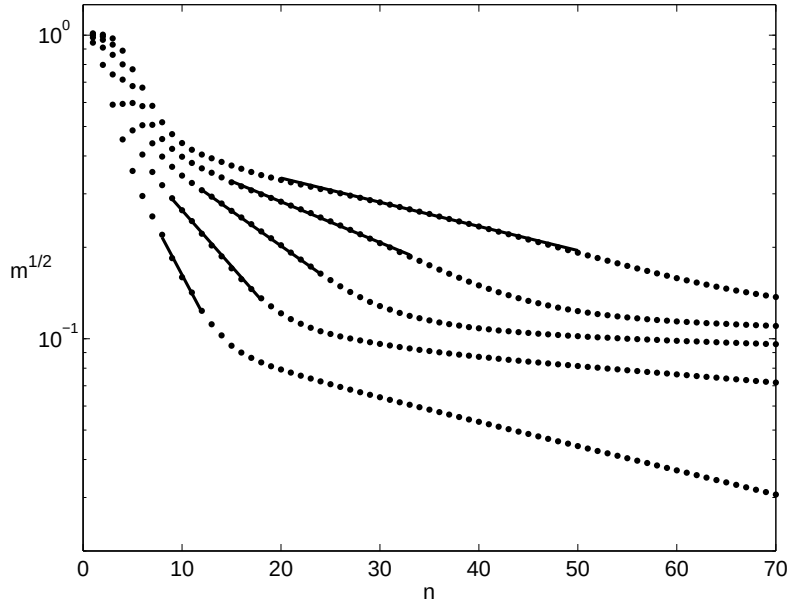

Figure 8: Mixing measures $m(n)$ for initial condition 1, for various Peclet numbers from 555 to 1.42×10^5. The Peclet number increases moving upwards among the curves. Exponential fits within the stirring interval are shown, the scaling of these fits is shown in Fig. 9.

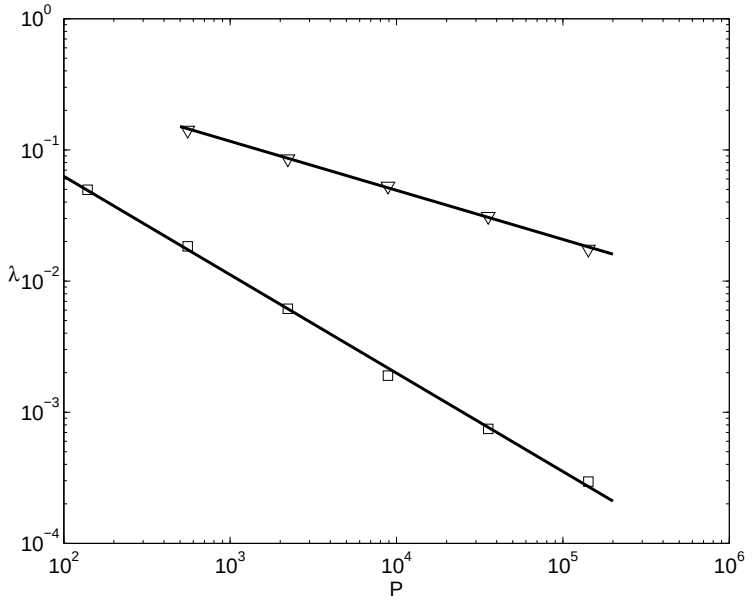

Figure 9: Scaling of the exponential fits $a\exp(-\lambda n)$ to the $m(n)$ curves. The triangles correspond to the stirring interval; the squares show the scaling of the long-time exponential decay rate. The fitted lines correspond to scalings of $P^{-0.37}$ (triangles) and $P^{-0.75}$ (squares).